Evaluation of Model-based Real-time Latency Compensation for Unmanned Aircraft Remote Control

Ole A. Ostermann*, Martin Laubner† and Sven Lorenz‡
DLR - German Aerospace Center, Braunschweig, 38108, Germany

For advanced flight testing of novel Unmanned Aircraft Systems (UAS) based on a synthetic vision, special skills and properties are required for direct First Person View (FPV) remote control. Necessary wireless data links and computer based data processing will introduce latency into the system. A UAS demonstration system has previously been built at the German Aerospace Center (DLR). For this system it was observed that the overall latency of the system reaches a magnitude where Pilot Induced Oscillation (PIO) occurs. In addition, bandwidth limitations result in low sampling rates in the downlink, leading to jerking flight information displays and visualizations. Due to those influences, handling qualities are fairly poor and will further decrease for Beyond Visual Line Of Sight (BVLOS) operations. To provide a pilot with smooth, accurate, and up-to-date visual cues, a compensation approach is developed that accounts for the full combination of: Delays, low sample rates, unavailable aircraft state measurements, modelling uncertainties, disturbances and sensor noises. An evaluation of three model-based methods is performed in this work, supported by a pilot-in-the-loop simulation test campaign. The measured accuracy of the compensated output as well as the subjective handling quality surveys show very promising results.

I. Nomenclature

$\boldsymbol{A}, \boldsymbol{B}, \boldsymbol{C}, \boldsymbol{D}$	=	state space system matrices
h	=	altitude
K	=	Kalman Filter gain
$\boldsymbol{P}$	=	state covariance estimate matrix
q	=	pitch rate
$\boldsymbol{Q}$	=	process noise power spectral density matrix
$\boldsymbol{R}$	=	measurement noise covariance matrix
z	=	complex frequency in Laplace domain
u, w	=	velocities (aircraft body, wind)
v	=	measurement noise
w	=	process noise
w_{Ri}	=	induced downwash velocity at rotor
$\boldsymbol{u}$, $\boldsymbol{x}$, $\boldsymbol{y}$	=	system input-, state- and output vector
$\hat{\boldsymbol{x}}, \hat{\boldsymbol{y}}$	=	estimated system states/outputs
x	=	geodetic position
α	=	aerodynamic angle of attack
β_{Blc}	=	maximum blade flapping angle
γ	=	flight path angle
δ_{TW}	=	thrust (engines)
$\delta(t)$	=	Dirac-Impulse
η_{RH}	=	rotor head steering angle
τ	=	delay time
θ	=	pitch angle
Ω_R	=	rotational speed of the rotor
Ω_{TW}	=	rotational speed of the engine

*Research Scientist, Institute of Flight Systems, ole.ostermann@dlr.de.
†Research Scientist, Institute of Flight Systems, martin.laubner@dlr.de.
‡Research Scientist, Institute of Flight Systems, sven.lorenz@dlr.de.

II. Introduction

First Person View (FPV) remote control capabilities are desired for flight testing of novel Unmanned Aircraft Systems (UAS) and can serve as a backup for prospective autonomous systems as well. The German Aerospace Center's (DLR) unmanned testbed ALAADy-Demonstrator [1], a 450 kg gyroplane, is a demonstrator for unmanned freight transportation, and is used as an example unmanned system for evaluation. In its FPV Ground Control Station (FPV-GCS), sensor-based synthetic vision is utilized in addition to a live, close to real time, video system. The testbed is shown in Figure 1 with the demonstrator aircraft on the left and a FPV-GCS setup on the right (live-video on the large upper screen and experimental synthetic vision on the bottom left screen). In future, the synthetic vision may replace the live-video system due to its following benefits:

- unrestricted field of view in arbitrary direction whereas cameras for live-videos are fixed in their installed location and demand a free direction of view,
- independence of visibility conditions (e.g. due to fog, rain, night, etc.),
- lower bandwidth requirements, particularly for future Beyond Visual Line Of Sight (BVLOS) applications (videos contain more data than pure sensor information),
- sensor information is typically available in a ground control station for monitoring, whereas live video requires additional data transmission,
- latency and bandwidth constraints might be easier to compensate for synthetic visualizations,
- and the ability to combine them with virtual reality systems for an even more immersive piloting experience.

(a) DLR's UAS gyroplane demonstrator **(b) FPV-GCS setup**

Fig. 1 ALAADy-Demonstrator

A wireless data link, that synthetic vision based remote control relies on, will introduce additional transmission delays into the system [1–4] (besides existing delays e.g. from computational processing). The delay has been observed to reach an order of magnitude of 100 ms in previous flight tests of the DLR's demonstrator system. This number might still increase specifically with new connection methods for BVLOS scenarios like cellular networks or satellite connections (the latter can suffer from delays up to the order of seconds) [1–4]. In addition, limited bandwidth leads to common sensor data sampling rates of only about 2 - 4 Hz in the downlink. This results in poor handling characteristics that can lead to Pilot Induced Oscillations (PIO) if direct control is implemented only. A compensation method is desired to provide the pilot with smooth, accurate and nearly up-to-date visual cues and thus reduce the danger of PIOs. Figure 2 presents a block diagram describing the problem and indicating where a compensation method will be applied.

Some latency or sample rate compensation approaches have been tested for remote control applications of aircraft [3, 4] or robots [5] in the recent past but to the knowledge of the authors the full combination of: Delays, low sample rates, unavailable aircraft state measurements, modelling uncertainties, disturbances (e.g. wind) and sensor noises has not been considered in literature yet. Therefore, three different methods are tested and compared against an undisturbed reference model as well as the emulated raw sensor measurements. The three tested methods are:

1) linear Kalman Filter (KF) with inherent wind estimation,
2a) the linear KF with an additional prediction by means of a Smith Predictor and
2b) the linear KF with an additional prediction by means of a "Recalculation".

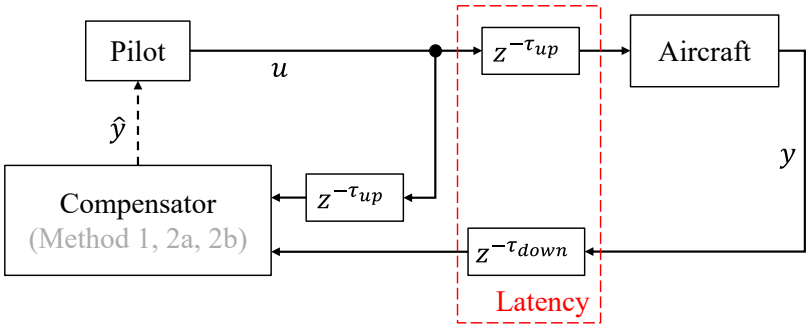

Fig. 2 Latency compensation scheme - block diagram

u - pilot control input, y - output (sensor measurements), $\hat{y}$ - compensated output estimations, τ - latency, *up* - uplink, *down* - downlink

The evaluation is supported by a pilot-in-the-loop simulation test campaign for which a handling quality survey and data recordings are analyzed. In summary, the objective of this work is to find a compensation method that provides the pilot with:

- Smooth and up-to-date synthetic visualizations,
- accurate flight information and
- copes with the full combination of impairments.

III. Flight Dynamics Model

For the fundamental comparison of different compensation methods and their resulting handling qualities it is deemed sufficient to only use the longitudinal model of the ALAADy-Demonstrator gyroplane which can be entirely separated from the lateral model [6]. The reduced complexity allows for a simpler implementation and analysis of different compensation methods. The non-linear 3-degrees-of-freedom model is implemented similarly to the explanations and relations in [6, 7].

In future applications with the real flying system, one may use the complete non-linear dynamics model of the aircraft for the model-based compensation methods. This model should resemble the real system sufficiently well. However, model uncertainties will always remain. Those are here described as process noise. For the technology exploration and evaluation of compensation methods for synthetic visualization in this paper, only models and simulations are used. It is thus decided to use the non-linear model as the "true" reference model and use only linearized and therefore further imperfect Linear Time Invariant (LTI) models for the model-based compensation methods. This artificially introduces more modelling errors compared to the non-linear model. Furthermore, it simplifies rapid implementation and analysis for this study.

The LTI state space model is represented by the system matrices $\boldsymbol{A}$, $\boldsymbol{B}$, $\boldsymbol{C}$, $\boldsymbol{D}$ (displayed in detail in the Appendix) as

$$\begin{aligned} \dot{\boldsymbol{x}} &= \boldsymbol{A}\,\boldsymbol{x} + \boldsymbol{B}\,\boldsymbol{u} \\ \boldsymbol{y} &= \boldsymbol{C}\,\boldsymbol{x} + \boldsymbol{D}\,\boldsymbol{u} \end{aligned} \tag{1}$$

with the input-, state- and output vectors $\boldsymbol{u}$, $\boldsymbol{x}$, $\boldsymbol{y}$ respectively described by

$$\begin{aligned} \boldsymbol{u} &= [\delta_{TW},\, \eta_{RH},\, u_{wind},\, w_{wind}]^{\mathsf{T}} \\ \boldsymbol{x} &= [\theta,\, w,\, u,\, w_{Ri},\, \Omega_R,\, \beta_{Blc\,Integrator},\, q,\, h,\, x]^{\mathsf{T}} \\ \boldsymbol{y} &= [\alpha,\, u,\, w,\, q,\, \theta,\, h,\, \gamma,\, V_{TAS},\, \Omega_{TW},\, \Omega_R,\, x]^{\mathsf{T}} \end{aligned} \tag{2}$$

for which the individual variables are described in Table 1.

Table 1 Description of inputs, states and outputs

δ_{TW}	η_{RH}	θ	u, w	w_{Ri}	Ω_R
thrust input	rotor head steering angle	pitch angle	velocity in x, z-direction	induced downwash vel. at rotor	rot. speed of the rotor

Ω_{TW}	β_{Blc}	q	x, h	α	γ
rot. speed of the engine	max. blade flapping angle	pitch rate	position /altitude	aerodynamic angle of attack	flight path angle

IV. Compensation Techniques

A. State Estimation and Filtering

State estimators, filters, or observers have proven to be a powerful tool especially in the area of sensor fusion for compensating for low sample rates, measurement noises and drift by utilizing an observable model of the system [5, 8, 9]. The Kalman Filter (KF) is a popular state estimator for which the controller gains of the observer are calculated iteratively based on knowledge and statistical Gaussian assumptions on the disturbances and noises in the system. Its least-squares approach yields the best linear estimator [8, 10]. The KF is computationally little demanding and recursive which allows real-time application. Kalman filters are kind of standard for the estimation of states in inertial navigation applications to compensate for measurement noises, modelling uncertainties, non-measurable states and low measurement update rates. Similarly to those sensor fusion applications, the filter may be used to mitigate these challenges in remote control applications. This has been shown for a virtual reality robot remote control problem in [5] for instance and is therefore also selected as a promising technique in this paper.

Assuming the availability of proper computing power for the synthetic vision in the FPV-GCS, the state space system can be handled in continuous time here, whereas the measurements inherently become available in discrete time. The hybrid (also called continuous-discrete) KF version can then be applied, which yields the advantage that measurements can be processed whenever they are received while in the absence of measurement updates, the filter continuously performs only predictions using its inherent model. This makes it very easy to handle irregular data transfer [8] as is expected for the downlink connection. This system can be represented by

$$\begin{aligned} \dot{\boldsymbol{x}}(t) &= \boldsymbol{A}\,\boldsymbol{x}(t) + \boldsymbol{B}\,\boldsymbol{u}(t) + \boldsymbol{w}(t) \\ \boldsymbol{y}_k &= \boldsymbol{C}_k\,\boldsymbol{x}_k + \boldsymbol{D}_k\,\boldsymbol{u}_k + \boldsymbol{v}_k \end{aligned} \tag{3}$$

where $\boldsymbol{x}_k = \boldsymbol{x}(t_k)$ and $\boldsymbol{x}_{k+1} = \boldsymbol{x}(t_{k+1})$. The vectors $\boldsymbol{w}$ and $\boldsymbol{v}_k$ are the process and measurement noise respectively. The measurement noise vector is defined as

$$\boldsymbol{v}_k \sim N\big(0,\ \boldsymbol{R}_k\big) \tag{4}$$

in discrete time with the covariance matrix $\boldsymbol{R}_k = E\big\{\boldsymbol{v}_k\,\boldsymbol{v}_k^{\mathsf{T}}\big\}$, $\boldsymbol{R}_k > 0$. The symbol E depicts the expected value. The process noise vector is similarly defined as

$$\boldsymbol{w}(t) \sim N\big(0,\ \boldsymbol{Q}(t)\big) \tag{5}$$

in continuous time [8, 9] with the power spectral density matrix defined in $\boldsymbol{Q}\,\delta(t - t_1) = E\big\{\boldsymbol{w}(t)\,\boldsymbol{w}(t_1)^{\mathsf{T}}\big\}$, $\boldsymbol{Q} \geq 0$ where $\delta(t - t_1)$ is the Dirac-Impulse.

The equations of the hybrid KF can be taken from textbooks like [8] and have been altered here to include the feed-through matrix $\boldsymbol{D}$. The KF state update calculation is divided into two steps:

1) The prediction step
2) and the correction step.

The prediction step calculates the a priori state estimate $\hat{\boldsymbol{x}}_{k|k-1} = \hat{\boldsymbol{x}}\,(t_k)$ and state covariance estimate $\boldsymbol{P}_{k|k-1} = \boldsymbol{P}\,(t_k)$ as

$$\begin{aligned} \dot{\hat{\boldsymbol{x}}}(t) &= \boldsymbol{A}(t)\,\hat{\boldsymbol{x}}(t) + \boldsymbol{B}(t)\,\boldsymbol{u}(t) \\ \dot{\boldsymbol{P}}(t) &= \boldsymbol{A}(t)\,\boldsymbol{P}(t) + \boldsymbol{P}(t)\,\boldsymbol{A}(t)^{\mathsf{T}} + \boldsymbol{Q}(t). \end{aligned} \tag{6}$$

The subscript "k|k-1" is resembling the Bayesian notation here and reads "k" given the evidence of "k-1". Equation 6 continuously predicts the system's state by using a representation of the system, in this case an LTI state space model

and estimates the confidence (covariance $\boldsymbol{P}$) in this prediction based on the covariance of the last time step (affected through the system dynamics) and our estimation of the process noise.

The correction step, also referred to as the measurement update, then uses the measurements from the real system $\boldsymbol{y}_k$ and the estimation of their accuracy (measurement noise covariance) as well as the state estimate $\hat{\boldsymbol{x}}_{k|k-1}$ together with the confidence (covariance $\boldsymbol{P}_{k|k-1}$) in it from the prediction step as

$$\begin{aligned} \boldsymbol{K}_k &= \boldsymbol{P}_{k|k-1}\boldsymbol{C}_k^{\mathsf{T}}\left(\boldsymbol{C}_k\,\boldsymbol{P}_{k|k-1}\,\boldsymbol{C}_k^{\mathsf{T}} + \boldsymbol{R}_k\right)^{-1} \\ \hat{\boldsymbol{x}}_k &= \hat{\boldsymbol{x}}_{k|k-1} + \boldsymbol{K}_k\left(\boldsymbol{y}_k - \boldsymbol{C}_k\,\hat{\boldsymbol{x}}_{k|k-1} - \boldsymbol{D}_k\,\boldsymbol{u}_k\right) \\ \boldsymbol{P}_k &= (\boldsymbol{I} - \boldsymbol{K}_k\,\boldsymbol{C}_k)\,\boldsymbol{P}_{k|k-1} \end{aligned} \tag{7}$$

to obtain the a posteriori state estimate $\hat{\boldsymbol{x}}_k$ and covariance estimate $\boldsymbol{P}_k$ - valid for the optimal Kalman gain $\boldsymbol{K}_k$. In case the assumptions of the process and measurement noises as Gaussian noise are incorrect, the Kalman gain diminishes from being the optimal gain to being the best linear estimator in which case the covariance estimate $\boldsymbol{P}_k$ instead has to be calculated according to the more complex Joseph form [8, 70,73], which is also more robust to roundoff errors - therefore preferred in software implementations - and is thus the one that is actually implemented in the corresponding Simulink® block by Mathworks Inc. [11]

$$\boldsymbol{P}_k = (\boldsymbol{I} - \boldsymbol{K}_k\,\boldsymbol{C}_k)\,\boldsymbol{P}_{k|k-1}\,(\boldsymbol{I} - \boldsymbol{K}_k\,\boldsymbol{C}_k)^{\mathsf{T}} + \boldsymbol{K}_k\,\boldsymbol{R}_k\,\boldsymbol{K}_k^{\mathsf{T}}. \tag{8}$$

In other words the correction step corrects the estimated state based on the measurements and the confidence in both measurements and prediction through a weighted average represented by the KF gain $\boldsymbol{K}_k$. The KF gain essentially minimizes the quadratic cost function [10]

$$\boldsymbol{J} = \lim_{t\to\infty} E\left\{(\boldsymbol{x}(t) - \hat{\boldsymbol{x}}(t))^{\mathsf{T}} \cdot (\boldsymbol{x}(t) - \hat{\boldsymbol{x}}(t))\right\} \tag{9}$$

The KF estimation will asymptotically converge (as quickly as desired) when the system is detectable (observable) [8] and when the dynamics of the KF's inherent model with the disturbance assumptions sufficiently match the dynamics of the actual system [12].

A special use case of KFs is the error state estimation [9]. It is a method for estimating anticipated deficiencies in the inherent model or external disturbances when it is known how they would affect the model while their quantities are unknown. For instance, it is common to estimate and correct inertial navigation system errors (like sensor drift) in sensor fusion algorithms or to estimate quantities like gravity or moments of inertia in space applications. By giving the KF a placeholder for disturbances in form of additional states and modeling how these would influence the model, the KF can better fit its inherent model's dynamics to the measurements and thereby the dynamics of the real system. It estimates the disturbances through the Kalman Gain. This estimation is subject to a delay which varies with the measurement update rate. In this work, the error state estimation method is applied for estimating wind disturbances as in [13]. The estimated wind could potentially be used also for surveillance purposes in future. However, the estimates have to be considered with caution, as the KF could project other errors such as delays or deviations from the estimated trim condition into the wind error states as well.

B. State Prediction

While the basic KF can help on filtering noises and modelling errors, estimating non-measurable states as well as smoothing data, a dedicated prediction is required to target the delay. Two different methods are considered:

1) The Smith Predictor
2) and a "Recalculation" method.

1. Smith Predictor

The Smith Predictor was originally developed specifically to cope with delays within a control loop and is exemplarily shown in Figure 3. It has been tested for delay compensation in UAS remote control in [4] while the approach had been adopted from online multiplayer video game technology. Downlink connection delays of 500 and 1000 ms were tested for a video quadcopter. Predicted roll-angles were used to artificially turn the FPV video image.

The Smith Predictor uses the output that is affected by transmission delays and executes two estimations in parallel ($\hat{G}$ with and without delay). The latter is running up to the present while the first one is artificially delayed by the same

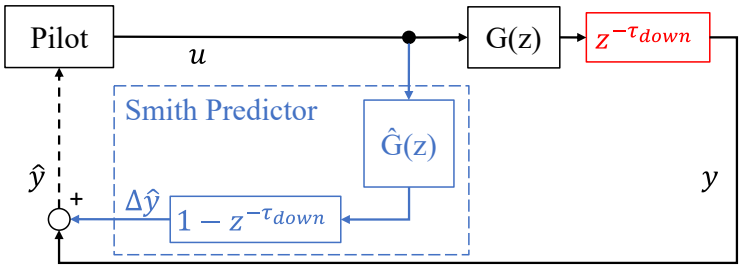

Fig. 3 Smith Predictor block diagram

$\Delta\hat{y}$ - predicted output estimate, $G(z)$ - real plant, $\hat{G}(z)$ - plant model, τ_{down} - downlink latency

time that the actual system is. This way the Smith Predictor continuously uses the actual system's output until the time it is available and interpolates from there to the present using the estimation. The inaccurate estimation is deducted for the time horizon for which real system measurements are available. This can be represented by

$$y = \left(G\, z^{-\tau_{down}} + \hat{G} - \hat{G}\, z^{-\tau_{down}}\right) u \tag{10}$$

where G represents the real system and $\hat{G}$ represents the model.

2. Recalculation

The "Recalculation" method is an alternative approach that has been tested with a Diamond DA42 aircraft model for compensation of remote control transmission delays using non-linear model-based prediction [3]. The principle is illustrated in Figure 4.

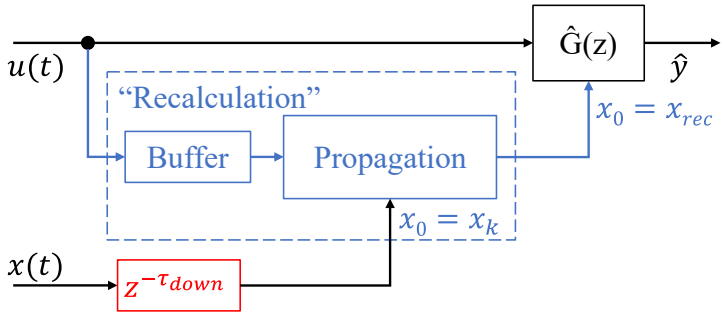

Fig. 4 Recalculation method block diagram illustration

The remote pilot flies in a synthetic vision simulation based on a model $\hat{G}$. The pilot's control input history is continuously stored in a sufficiently long buffer. Each time a measurement update arrives, a recalculation is triggered: The buffered control input history is utilised together with a state vector that must be obtained from the new measurements, to initialize and propagate a separate model from the time at which the measurement was taken until the present (which is essentially the delay time). The output of this propagation is then used to periodically reset/correct the synthetic vision simulation.

V. Evaluation Setup

A. Combination of Methods and Implementation

For this evaluation of model-based real-time latency compensation, the linear KF with wind estimation is chosen as basic filter. The through the KF yet unresolved pure delay can then either be neglected because it is still expected to be small (*Method 1*) or it can be separately addressed by an additional prediction method (*Method 2*). In these cases the compensation method can be described as a two-step process. The first step consists of the KF that receives the

transmission-delayed measurements plus the pilot control inputs which are artificially delayed by the same downlink delay time. All inputs are thus received in a time-consistent manner and the KF is executed using this data from the past. In the second step, the estimated, continuous states from the KF are then used for an additional prediction to specifically target the downlink delay. This is achieved by making use of the remaining time history of the pilot control input.

For this prediction, the "Recalculation" method seemed to deliver more accurate results through the complete reset of the synthetic vision simulation after each measurement update & propagation but therefore provides less smooth outputs than the simpler Smith Predictor. Both methods are therefore selected for further testing (*Method 2a* and *2b*), resulting in essentially 3 different methods to be tested in the flight simulation campaign.

In contrary to the KF, the prediction methods are not possible to be used alone as they are not able to handle the remarkably low sample rates. Additionally, disturbances and noises could not be sufficiently compensated either. The "Recalculation" method requires knowledge about the full state vector and would thus require some state observer anyway because not all states are measurable with this aircraft model.

The inputs, states and outputs (compare with Equation 2) that are applied for the KF are:

$$\begin{aligned} \boldsymbol{u}_{KF} &= [\delta_{TW},\, \eta_{RH}]^\mathsf{T} \\ \boldsymbol{x}_{KF} &= [\theta,\, w,\, u,\, w_{Ri},\, \Omega_R,\, \beta_{Blc\,Integrator},\, q,\, h,\, x,\, w_{wind},\, u_{wind}]^\mathsf{T} \\ \boldsymbol{y}_{KF} &= [\alpha,\, u,\, w,\, \theta,\, h,\, V_{TAS},\, \Omega_R,\, x]^\mathsf{T}. \end{aligned} \tag{11}$$

Measurements of the rotation speed of the engine Ω_{TW}, the pitch rate q and the flight path angle γ are not made available for the KF in order to see how it handles a limited number of outputs. Nevertheless, the resulting LTI model remains observable. Especially the pitch rate has a comparably high noise to signal ratio particularly for gyroplanes due to the oscillations of the rotor. Therefore its inclusion provides no benefit to the KF (already receiving the pitch angle θ) and is disregarded. Theoretically a reduction of the number of utilized outputs could also reduce the required bandwidth and therefore increase the measurement sample rate for the downlink in future. This would require further investigation because a lower number of outputs would decrease the KF's accuracy while a higher sample rate would significantly increase it. The presented selection of outputs is in-line with the readily available data in the existing downlink of the DLR's ALAADy-Demonstrator. The noise characteristics in this evaluation are modelled in conservative accordance with previous flight test log files. Possible covariances in the measurement noises due to periodic vibrations from the rotor are not accounted for so far.

The state vector for the KF model has two additional states for the wind estimations and the input vector does not have wind inputs (because it is unknown). It was observed that the wind estimation is strongly dependent on the measurement's sample rate. It works very well with continuous measurements while its precision significantly decreases with lower update rates. Especially after extending the methods to lateral dynamics and potentially non-linear models, a reevaluation of the wind estimation technique is advised.

The initial conditions will probably never be known exactly in reality, which is why a deviation is also added to the initial condition vector $x_{KF,0}$ of the KF here (rad for angles and rotations and meter for velocities and positions) as

$$\boldsymbol{x}_{KF,0} = \; [0.001,\, 0.1,\, -0.3,\, 0.1,\, -0.5,\, 0,\, 0,\, 0.1,\, 0.1,\, 0.1,\, 0.1]^\mathsf{T}. \tag{12}$$

Initial condition errors of e.g. -0.3 m/s for the aircraft flight speed shall prove that the implemented KF is robust. In fact, as an additional error, the LTI model for the considered horizontal wings-level flight at 90 km/h is actually trimmed with a descent velocity of 0.1 m/s.

The process noise is difficult to estimate because inaccuracies of the flight dynamics model are typically not perfectly known. Estimations are commonly made empirically by means of tuning campaigns to adjust the entries of the power spectral density matrix $\boldsymbol{Q}$ defined in Equation 5. For the real system implementation a possibility would be to conduct extensive flight test campaigns and compare the measurements with corresponding simulations [9]. The adjustment of the process noise characterization in the KF (in $\boldsymbol{Q}$) could then be handled as an optimization problem that seeks to minimize the error between real-world measurements and simulated outputs. This was actually done in this study using the non-linear model as the reference and comparing it to the LTI model. A mathematical optimization was utilized to obtain some first indications of the entries in the power spectral density matrix $\boldsymbol{Q}$. Further fine-tuning was executed manually to achieve a balance of accuracy over smoothness. The utilized noise matrices are shown in Equation 13. Although there will most certainly be cross correlations between the different states they were neglected to not overburden this optimization problem for the first evaluation in this project and leaving room for further optimizing the KF. Cross correlations are also indirectly introduced through the calculation of the state covariance estimate $\boldsymbol{P}$ by multiplication with the state transition matrix $\boldsymbol{A}$ in the prediction step (Equation 6).

$$
\begin{aligned}
\boldsymbol{R} &= \text{diag}(0.0087,\ 0.005,\ 0.005,\ 0.0003,\ 0.02,\ 0.02,\ 0.5,\ 0.02) \\
\boldsymbol{Q}_{KF1} &= \text{diag}(1\text{e-}5,\ 1,\ 1,\ 1\text{e-}5,\ 1\text{e-}5,\ 1\text{e-}5,\ 0.5,\ 10,\ 10,\ 50,\ 50) \\
\boldsymbol{Q}_{KF2} &= \text{diag}(1\text{e-}5,\ 1,\ 1,\ 1\text{e-}5,\ 1\text{e-}5,\ 1\text{e-}5,\ 5,\ 10,\ 10,\ 25,\ 25)
\end{aligned} \tag{13}
$$

B. Simulation Test Campaign Setup

To investigate the effects of each compensation method with different delays and different available measurement update rates on the handling qualities of the aircraft, pilot in the loop flight simulation tests were conducted. A non-linear undisturbed model of the ALAADy-Demonstrator's longitudinal motion is used as the reference model for comparison. The final flight simulation campaign test setup with a desktop computer is shown in Figure 5. On the right, a visualization is shown in-flight above the runway of the Brunswick research airport with images from Cesium®. The black flight information HUD is laid on top. A velocity indicator for the true airspeed V_{TAS} was given on the left together with a percentage for the engine input. A basic consumer joystick was used that has a small built-in throttle lever.

Fig. 5 Test campaign setup

A number of nine candidates were recruited as test pilots. Three candidates are licensed pilots. One has experience on gyroplanes, one flies various general aviation and aerobatics aircraft and one is trained on airliner aircraft. The majority of candidates had flown in flight simulations before, some of them regularly on the proper gyroplane flight simulator at the DLR. Two of the candidates performed the tests twice with a break of more than one week in between. The results of those two candidates were used to analyse consistency and validity of the handling quality survey. This amounts to a total number of eleven flight test runs for a latency setting of 200 ms and 4 Hz sample rate. For a brief outlook and comparison three of the candidates were available to additionally fly the tests with a latency setting of 400 ms and 2 Hz update rate. After each tested compensation method the pilots were asked to subjectively rate the handling qualities.

For the simulation flight test mission it was chosen to prescribe an altitude profile to be followed by the pilots (outlined in Table 2) while being exposed to modest wind disturbances, sensor noises, latency and low sample rates. Before starting the flight tests, each candidate was given some time to familiarize themselves with the gyroplane's flight dynamics, the visualization setup and the flight mission. This training was performed with the non-linear reference model. Depending on the candidate's experience it was needed to specifically get used to the interactions between rotor head angle control, pitch angle, airspeed and thrust. At last, another final training flight was conducted using only the emulated raw measurement data (subject to latency and noises) for visualization. This gave the pilots an idea of the worst-case scenario so that they could later evaluate the different compensation methods relatively. The wind profile was varied randomly for the training.

Table 2 Mission: Altitude above ground flight tasks

time period [s]	Start	0 - 40	40 - 80	80 - 120
height [ft]	330	300	330	400

Working solely with longitudinal dynamics, vertical disturbances are introduced that push the aircraft off the demanded altitude. This shall urge the pilots to do control inputs which is required to evaluate the danger of PIOs as well as the ability of the pilots to follow the flight plan despite disturbances. A simple sequence of vertical wind was modeled to resemble gusts. The wind velocity is changed every 5 seconds. To obtain a smooth and more realistic wind profile the discrete wind profile is low-pass filtered. This can be seen later in the results in Figure 8. During the campaign the wind profile was kept the same for all test flights. This poses the danger that pilots can possibly memorize the wind pattern after a while. On the other hand, the wind pattern heavily influences the pilot's performance. To give an example, it is much more difficult to reach a demanded altitude when a heavy gust occurs during the climb. Pilots often either struggle to keep the airspeed and climb rate or substantially overshoot the demanded altitude. To compare different latency compensation methods and to validate the pilots performance with them against the original non-linear model, it is thus beneficial to keep the wind profile the same for all tests. The training effect of memorizing the wind's pattern is statistically mitigated by letting each pilot fly the different models and compensation methods in a different order.

VI. Results

The analysis of the flight simulation tests with visualized outputs of the five different methods/models (undisturbed non-linear reference model, emulated raw measurements, *Method 1* with a pure KF, *Method 2a* with a KF plus Smith Predictor and *Method 2b* with a KF plus "Recalculation") is divided into 3 aspects:

(A) The performance of the pilot to fulfill the flight mission,
(B) the performance of the methods to accurately and smoothly estimate the real/reference system states in order to provide the pilot with a truthful and consistent visual of the aircraft,
(C) and lastly the subjective assessment of the handling qualities by the pilots themselves.

A. Pilot Performance

The deviations of the altitude from flight plan were the primary focus of the flight mission for the pilots. Considered are the time averages of the Median, the Mean and the Standard Deviation (SD) of the candidates at each time step. The results are shown in Figure 6. The uncompensated raw measurements were the most difficult to fly with and the original undelayed reference model visualizations showed the best results which both meet the expectations and thus serves as validation of the results. Compared to the raw measurements, all compensation methods enhanced the experience for the candidates enabling them to perform better. The statistical parameters are lying in between measurements and reference model. The methods with prediction are superior to the pure KF method when looking at the median. Results are yet relatively close to each other and should therefore rather be taken as indications. It has to be noted that the candidates had a limited average skill level and were only given limited time to train with the somewhat unusual flight dynamics of the gyroplane. However, the median is less sensitive to individual candidate failures and the analysis is supported by the test runs with stronger latency settings which show the same trend but significantly more pronounced.

B. Compensation Method Performance/Accuracy

Similarly to the pilot performance analysis, time averages of the median, mean and mean with standard deviation of the different test runs are calculated for the output errors. The output errors are the differences between the compensation method outputs that are shown to the pilot and the output of the reference model that was simulated in parallel with the same input (obviously including the same uplink delay). As an example, the errors for the altitude are shown in Figure 7. Performance errors for other relevant variables e.g. the pitch angle look very similar.

Stronger latencies lead to worse performances for all methods as expected. The compensation methods performed substantially better in both latency settings compared to raw measurements for which errors were more than twice as high. The prediction methods both outperformed the pure KF implementation, while the "Recalculation" method performed best with a slight margin.

1. Wind Estimation

Wind estimation results are similar for Method 2a and 2b because they use the same KF constellation, whereas estimations with Method 1 are different. Results are exemplary shown for the Smith Predictor method tests in Figure 8. Displayed are the vertical wind estimates of all test runs for the 200 ms and 4 Hz scenario as dotted lines where each color describes one pilot recording. The true wind is shown with the red curve. The wind pattern is estimated mostly accurate but with a delay of around one second which is best visible whenever the wind changes are very sudden.

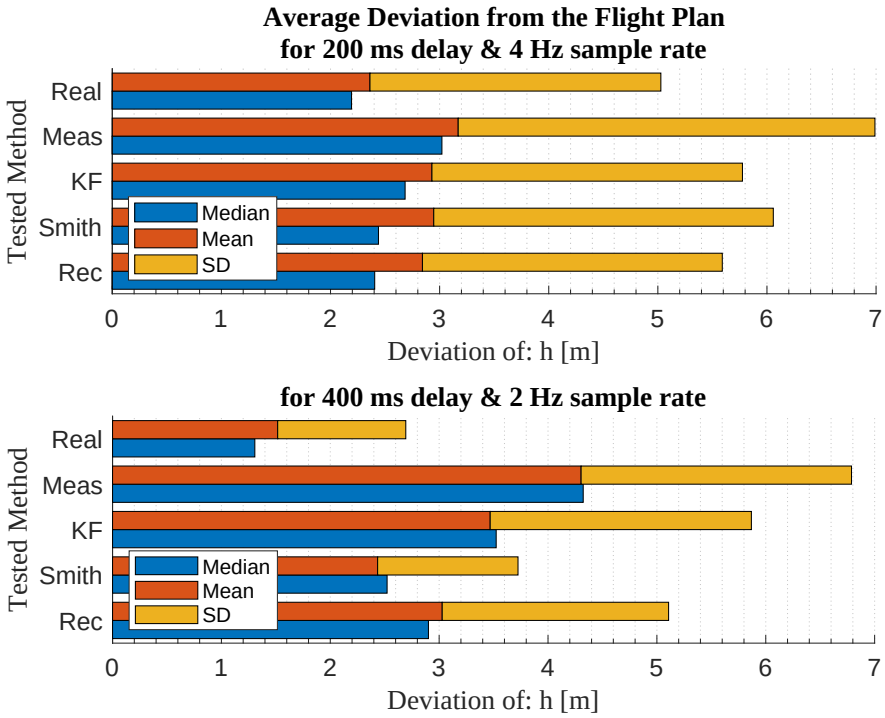

Fig. 6 Average Flight Plan Deviations (over the last 20 s of each demanded altitude)

SD - standard deviation, *Real* - non-linear undelayed reference model, *Meas* - emulated raw measurements, *KF* - Kalman Filter (Method 1), *Smith* - KF + Smith Prediction (Method 2a), *Rec* - KF + Recalculation (Method 2b)

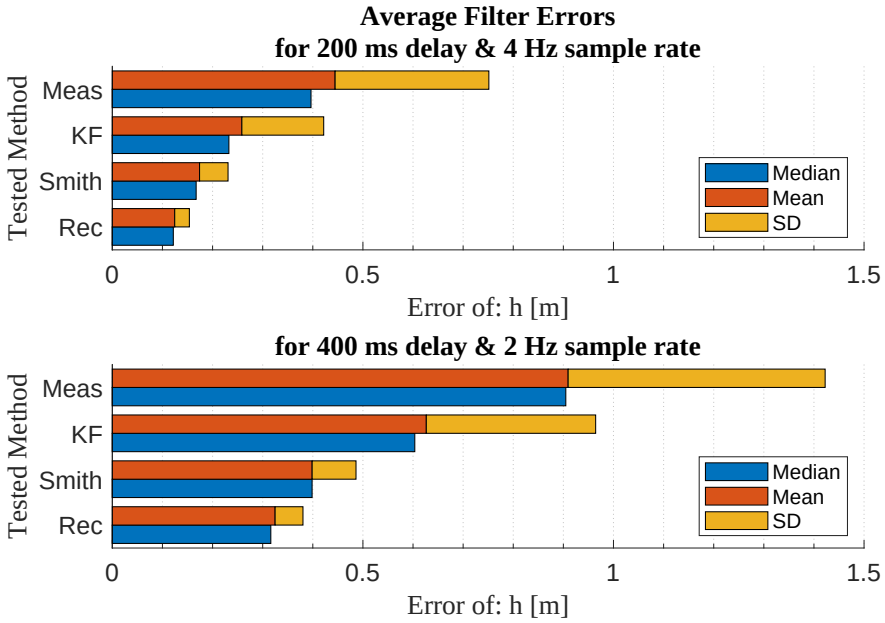

Fig. 7 Filter Errors Average - Altitude

Investigations showed that individual/local outruns (e.g. at around 90 s) coincided with increasing output errors at the same time and for the same candidates. By comparison with pure linear model outputs (that were simultaneously recorded during the campaign), they were discovered to result from validity limitations of the linearized model when

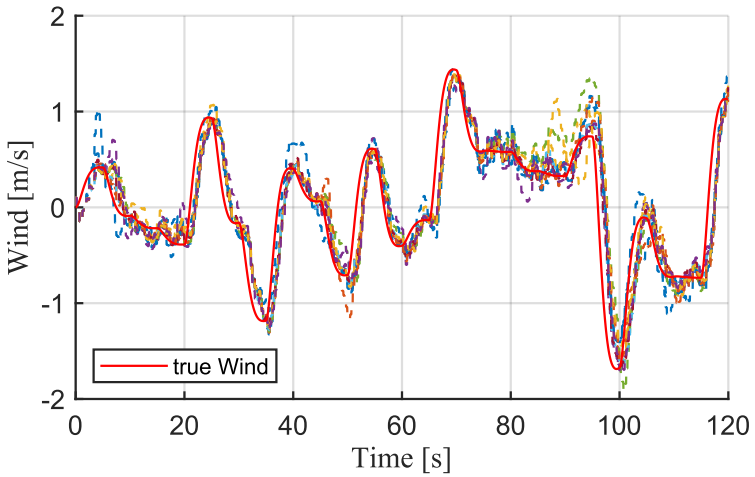

Fig. 8 Wind estimation: Smith Prediction Method - 4 Hz and 200 ms, (one color per pilot)

very low flight speeds are reached. It is thus expected that compensation method accuracies (including wind estimation) can be significantly improved further by accounting for non-linearities in future (through enhancement of compensation methods e.g. adaptive or extended KF). Estimations were significantly more noisy with only the pure KF (*Method 1*).

C. Pilot Evaluations

Pilot evaluation results are shown in Table 3. Inquired were ratings on the overall handling qualities (scale: 1-10), the ability to observe the state of the aircraft from the visualization ("observability", scale: 1-4) and how fast the aircraft appeared to respond to their control inputs ("responsibility", scale: 1-4). The lowest number always translates as "worst" and the highest number translates as "best". The latency compensation methods are rated slightly lower compared to the undisturbed non-linear reference model without latencies which is expected. However, they are all assessed substantially better than the usage of only the raw uncompensated measurements in all aspects. In-between the compensation methods, the recalculation method performed overall worse from the pilots point of view. Here, even the responsiveness is valued less than the pure KF which might be the result of the strong corrections due to the low sample rate which gives the pilot a subjective feeling of slower control input response because it is harder to observe. The other two methods gave very good results in the opinion of the pilots.

Table 3 Handling Qualities Survey Results (Averages)

Latency Settings	**Method**	**Overall Handling Qualities** (1-10)	**Observability** (1-4)	**Responsiveness** (1-4)
4 Hz & 200 ms	Non-linear Model	8.4	3.6	3.5
	Raw Measurements	3.5	1.9	1.3
	Kalman Filter	7	3.3	2.9
	KF + Smith Prediction	7.7	3.4	3.3
	KF + Recalculation	7.1	2.9	3.1
2 Hz & 400 ms	Non-linear Model	8.3	3.7	3.7
	Raw Measurements	2.7	1.3	1.7
	Kalman Filter	7	3.3	3
	KF + Smith Prediction	8	3.7	3.3
	KF + Recalculation	6.3	2.7	2.7

A rating with "1" translates as "worst", the highest number translates as "best". Please note that the rating scales are standalone and not related to the Cooper–Harper rating scale.

VII. Summary and Conclusion

The target of this work was a technology exploration and evaluation of model-based latency compensation methods for FPV remote control which account for the full combination of: Measurement transmission delays, low sample rates, unavailable aircraft state measurements, modelling uncertainties, (wind) disturbances and sensor noises. The methods were selected from examples in literature on sensor fusion as well as robot and aircraft remote control which focused on different subsets of the combination of impairments. A hybrid KF with wind estimation as well as its combination with two different prediction methods were investigated further in a flight simulation test campaign. The longitudinal flight dynamics model of the ALAADy-Demonstrator UAS, a 500kg weighing gyroplane from the DLR, served as an example. Based on a pilot evaluation and the recorded data from the flight simulations, an analysis of the improvement of handling qualities as well as the sensitivity to latency and update rate is performed, with a focus on the accuracy of the method's outputs.

The results of this study show a remarkable improvement of the synthetic visualizations for FPV remote control through model-based latency compensation. All methods are substantially better than the usage of the emulated raw measurements in all evaluated aspects: Errors to the real flight condition, pilot flight mission performance and the handling quality assessment through a survey. The KF in combination with an additional, separate prediction method delivers most suitable results. The "Recalculation" approach achieves slightly higher accuracy but is rated inferior by the pilots due to its less smooth output. In conclusion, the authors suggest the Smith Prediction method for future application because it is similarly accurate but also provides a very smooth output. This gives the pilots a subjective feeling that almost reaches the undisturbed non-linear model - even for the more severe delay & sample rate combination.

Appendix

A. LTI State Space System Matrices

$$\boldsymbol{A} = \begin{bmatrix} 0 & 0 & 0 & 0 & 0 & 0 & 1 & 0 & 0 \\ 25.74 & -1.277 & -0.1227 & 1.146 & -0.5446 & -25.75 & 24.84 & 0 & 0 \\ 3.518 & -0.1829 & -0.1596 & 0.175 & -0.05926 & -13.33 & -0.04412 & 0 & 0 \\ -161.6 & 6.869 & -1.499 & -36.87 & 3.247 & 161.6 & 0 & 0 & 0 \\ -16.59 & 0.7055 & 0.1164 & -0.7053 & -0.0446 & 16.59 & 0 & 0 & 0 \\ 9.456 & 0 & 0 & 0 & 0 & -9.456 & 0 & 0 & 0 \\ -13.47 & -0.03917 & 0.06042 & -0.07675 & 0.006578 & 13.47 & -0.1972 & 0 & 0 \\ -25 & 1 & -0.001776 & 0 & 0 & 0 & 0 & 0 & 0 \\ -1.2e\text{-}10 & 0.001776 & 1 & 0 & 0 & 0 & 0 & 0 & 0 \end{bmatrix}$$

$$\boldsymbol{B} = \begin{bmatrix} 0 & 0 & 0 & 0 \\ 0 & -1.618 & 0.125 & 1.277 \\ 0.01347 & -0.8376 & 0.1599 & 0.1827 \\ 0 & 10.16 & 1.487 & -6.872 \\ 0 & 1.043 & -0.1177 & -0.7053 \\ 0 & 9.456 & 0 & 0 \\ -0.003701 & 0.8464 & -0.06035 & 0.03928 \\ 0 & 0 & 0 & 0 \\ 0 & 0 & 0 & 0 \end{bmatrix}$$

$$\boldsymbol{C} = \begin{bmatrix} 0 & 0.04 & -7.103\text{e-}05 & 0 & 0 & 0 & 0 & 0 & 0 \\ -1.2\text{e-}10 & 0.001776 & 1 & 0 & 0 & 0 & 0 & 0 & 0 \\ -25 & 1 & -0.001776 & 0 & 0 & 0 & 0 & 0 & 0 \\ 0 & 0 & 0 & 0 & 0 & 0 & 1 & 0 & 0 \\ 1 & 0 & 0 & 0 & 0 & 0 & 0 & 0 & 0 \\ 0 & 0 & 0 & 0 & 0 & 0 & 0 & -1 & 0 \\ 1 & -0.04 & 7.103\text{e-}05 & 0 & 0 & 0 & 0 & 0 & 0 \\ 0 & 0.001776 & 1 & 0 & 0 & 0 & 0 & 0 & 0 \\ 0 & 0 & 0 & 0 & 0 & 0 & 0 & 0 & 0 \\ 0 & 0 & 0 & 0 & 1 & 0 & 0 & 0 & 0 \\ 0 & 0 & 0 & 0 & 0 & 0 & 0 & 0 & 1 \end{bmatrix}, \quad \boldsymbol{D} = \begin{bmatrix} 0 & 0 & 8.346\text{e-}15 & -0.04 \\ 0 & 0 & 0 & 0 \\ 0 & 0 & 0 & 0 \\ 0 & 0 & 0 & 0 \\ 0 & 0 & 0 & 0 \\ 0 & 0 & 0 & 0 \\ 0 & 0 & 0 & 0 \\ 0 & 0 & -1 & 1.183\text{e-}14 \\ 1 & 0 & 0 & 0 \\ 0 & 0 & 0 & 0 \\ 0 & 0 & 0 & 0 \end{bmatrix}$$

References

[1] Dauer, J. C. (ed.), *Automated Low-Altitude Air Delivery: Towards Autonomous Cargo Transportation with Drones*, Springer, 2022.

[2] Schalk, L. M., "Communication links for Unmanned Aircraft Systems in very low level airspace," *2017 Integrated Communications, Navigation and Surveillance Conference (ICNS)*, 2017, pp. 6B2–1–6B2–11. https://doi.org/10.1109/ICNSURV.2017.8011939.

[3] Zhang, F., Fricke, T., and Holzapfel, F., "Integrated Control and Display Augmentation for Manual Remote Flight Control in the Presence of Large Latency," *AIAA Guidance, Navigation, and Control Conference*, AIAA, 2016. https://doi.org/10.2514/6.2016-1867.

[4] Cox, J., and Wong, K., "Predictive feedback augmentation for manual control of an unmanned aerial vehicle with latency," *International Journal of Micro Air Vehicles*, Vol. 11: 1-9, 2019. https://doi.org/10.1177/1756829319869645.

[5] XuXiao, M., "Eliminating the latency using different Kalman filters: for a virtual reality based teleoperation system," Master's thesis, KTH, School of Computer Science and Communication (CSC), 2016. URL http://www.diva-portal.se/smash/get/diva2:943400/FULLTEXT01.pdf.

[6] Torgerson, J. F., "Simulation and control design of a gliding autogyro for precision airdrop," Master's thesis, Massachusetts Institute of Technology, 2005. URL https://dspace.mit.edu/handle/1721.1/32456.

[7] Duda, H., and Seewald, J., *Flugphysik der Tragschrauber*, Springer, 2017.

[8] Lewis, F. L., Xie, L., and Popa, D., *Optimal and Robust Estimation*, 2nd ed., CRC Press, 2008.

[9] Wendel, J., *Integrierte Navigationssysteme*, Oldenbourg Wissenschaftsverlag, 2007.

[10] Duriez, T., Brunton, S., and Noack, B., *Machine Learning Control – Taming Nonlinear Dynamics and Turbulence*, Springer, 2017, Vol. 116, Chap. Methods of Linear Control Theory, pp. 49–68. https://doi.org/10.1007/978-3-319-40624-4_3.

[11] *Matlab&Simulink: Documentation*, The MathWorks, Inc, Natick, MA, USA, 2021. URL https://mathworks.com/help/releases/R2021b/index.html.

[12] Brunton, S. L., and Kutz, J. N., *Data Driven Science & Engineering Machine Learning, Dynamical Systems, and Control*, Cambridge University Press, 2019.

[13] Wasim, M., Ali, A., Choudhry, M. A., Saleem, F., Shaikh, I. U. H., and Iqbal, J., "Unscented Kalman filter for airship model uncertainties and wind disturbance estimation," *PLOS ONE*, Vol. 16, No. 11, 2021. https://doi.org/10.1371/journal.pone.0257849.